CFD Letters www.cfdl.issres.net Vol. 3 (2) – June 2011

Coupled Coating Formation Simulation in Thermal Spray Processes using CFD and FEM

J. Prehm[C], L. Xin, K. Möhwald, Fr.-W. Bach
Institute of Materials Science , Leibniz University Hannover
GERMANY

Received: 10/11/2010 – Revised 24/12/2010 – Accepted 23/06/2011

Abstract

This paper deals with the simulation of coating formation in Thermal Spray processes. That means that impingement and flattening of molten metal- or ceramic particles with a diameter of about 50 microns on a rough surface have to be regarded. In this work, this is accomplished use of the Volume of Fluid method. The disadvantage here is that only the pure flattening process can be considered. In order to implicate the shrinking of the particles due to cooling down after solidification, which is responsible for the occurrence of pores and thermal stresses, a Finite Element calculation is done subsequent to the CFD-calculation. After the FEM calculation has finished, the newly generated, shrinked particle shape has to be re-imported into the CFD grid.

Keywords: Thermal Spraying, atmospheric plasma spraying, simulation, coating formation, Volume of Fluid method, particle spreading, pore formation

1. Introduction

The aim of this work is to simulate coating formation in the field of thermal spray processes. Here, mainly the atmospheric plasma spray process is regarded. In atmospheric plasma spraying (APS), the spraying particles are applied onto the substrate, in order to provide a coating. This is done by use of a plasma beam. To realize this plasma beam, an arc between the cathode and anode is generated in the so-called plasma torch. In the hottest zone of the plasma cone, temperatures of about 30000 K occur. The coating material in form of powder is injected into this plasma beam, where it is rapidly heated, molten and accelerated. Depending on the chosen process parameters, the powder particles impinge at a certain speed and temperature on the substrate.

Most of the previous simulations concerning this kind of coating formation can be divided into two categories: The first category covers simulations with which the impact and the spreading of molten particles on the substrate were calculated with the "Volume of fluid" (VOF) method [6]. One disadvantage here is, that the number of particle impacts is limited in these cases a few dozen, because of the extremely high computation time. The mean influence of parameters e.g. particle and substrate temperature, particle size as well as impact velocity and angle were examined in various publications [4, 13]. Meanwhile rough substrates are also taken into account [9], while in earlier simulations merely the impact onto flat substrates was investigated. In the second category

[C] Corresponding Author: Jens Prehm
Email: prehm@iw.uni-hannover.de
 PII: S2180-1363(11)3289-X

stochastic models were used in order to simulate coating formation. Here, neither the impact of single particles nor their solidification were computed. Instead of this, the form of the impacted particles was given on the basis of micrographs of coatings or previous simulations of particle impacts [3, 10]. With such statistical techniques several hundred particles can be included into the modelling of the coating formation. All the above mentioned models are not capable to compute porosities. If necessary they must be integrated into the model, later. Apart from simulations which regard only the coating structure, also procedures exist, which try to precalculate the mechanical behaviour of the thermal sprayed coating. For this, the Finite Element Method (FEM) is used. The input data for such simulations is normally gathered from micrographs or measurements. Since porosity is a characteristic property of thermal sprayed coatings, the pore formation plays a central role within the simulation of the coating formation [15]. Therefore, this article describes a method which allows to compute both, the flattening (with help of CFD) process and the subsequent cooling down process (with help of FEM), which is responsible for the shrinkage of the particles.

2. Approach

2.1. CFD Modelling

2.1.1. The Volume of Fluid Model

At first, the impact, the spreading and the solidification of a molten particle on the substrate are computed with CFD. Here, the volume of fluid algorithm (VOF) is used, which determines the free surface of the particle in the computational grid, time-resolved.

In our calculations we use a two phase VOF-Model. The primary phase is the surrounding gas (air), while the secondary phase consists of the molten particle.

For the volume fraction of a particle in a cell of the computational grid, the following can be obtained:

$\alpha_p = 0$: the cell contains no fluid (particle fraction)

$\alpha_p = 1$: the cell filled with fluid

$0 < \alpha_p < 1$: the cell contains an interface between particle and gas

The transport equation of this volume fraction is calculated via the following conservation equation:

$$\frac{1}{\rho_p}\left[\frac{\partial}{\partial t}(\alpha_p \rho_p) + \nabla(\alpha_p \rho_p \vec{v}_p) = 0\right] \tag{1}$$

The volume fraction of the primary phase - i.e. the gas - follows as:

$$\alpha_p + \alpha_g = 1 \tag{2}$$

In order to discretize equation (1) an implicit scheme is used [5]:

$$\frac{\alpha_p^{n+1}\rho_p^{n+1} - \alpha_p^n \rho_p^n}{\Delta t} V + \sum_f (\rho_p^{n+1} U_f^{n+1} \alpha_{p,f}^{n+1}) = 0 \tag{3}$$

A single momentum equation is solved throughout the domain, and the resulting velocity field is shared among the phases. The momentum equation, shown below, is dependent on the volume fractions of all phases through the properties ρ and μ.

The VOF model treats energy, E, and temperature, T, as mass-averaged variables:

$$E = (\alpha_g \rho_g E_g + \alpha_p \rho_p E_p) / (\alpha_g \rho_g + \alpha_p \rho_p) \tag{4}$$

where E_q for each phase is based on the specific heat of that phase and the shared temperature. The properties ρ_{eff} and λ_{eff} (effective density and effective thermal conductivity) are shared by the phases. The density is calculated as:

$$\rho_{eff} = \alpha_p \rho_p + (1-\alpha_g) \rho_g , \tag{5}$$

whereas the effective thermal conductivity is obtained by:

$$\lambda_{eff} = \alpha_p \lambda_p + (1-\alpha_g) \lambda_g \tag{6}$$

The energy equation is:

$$\frac{\partial}{\partial t}(\rho_{eff} E) + \nabla (\vec{v} (\rho_{eff} E + p)) = -\nabla \left[\lambda_{eff} \nabla T \right] \tag{7}$$

As indicated above, a solidification model is implemented in the VOF method [11, 12].

2.1.2. Geometry and physical properties of the model

At Thermal Spray processes the surface, that is to be coated, is roughened by use of grid blasting. That means that corundum particles with defined size fractions are blasted to the substrate. In order to consider this approach in the simulations, an algorithm which can take into account the deformation of the surface due to the impact of the shot during grid blasting was developed. In this model the form, the diameter, the depth of penetration and the quantity of the shot can be varied. Moreover a specific attenuation factor is integrated in the model. By help of Laser Scanning Microscope analysis, witch has a spacial resolution of about 1 nm, it is possible to measure the roughness of grid blasted surfaces space-resolved. Hence the simulated surface topologies can be attuned to reality. The so measured roughness peaks are about 30 μm. Fig. 1 shows a simulated surface topology of the substrate.

The basic material of this substrate is steel (1.0037), while for the spraying particles a ceramic is used. Here alumina goes into action, because it is a widely used coating material in the fields of corrosion protection and thermal barrier coatings. In the following calculations the steel substrate has an initial temperature of about 400 K, while the temperature of the alumina particles is about 2400 K. This means, that the melting temperature of alumina (approximately 2323 K) is exceeded and that the individual alumina particles are molten, so that they can be treated as a fluid in the CFD simulation. As temperature dependent properties of liquid alumina the following variables were used: density, specific heat, conductivity, surface tension and as a very important issue concerning the flattening process, the viscosity. Moreover the latent heat is integrated into

the model. The temperature dependent surface tension of liquid alumina is taken from the following formula [17]:

$$\sigma(T) = 0.64 - 8.2 \cdot 10^{-5} \, (T - T_m) \tag{8}$$

This formula is based on surface tension measurements in the temperature range of 2190 K to 2500 K.

The surrounding gas is treated as air with the temperature dependent properties of an ideal gas. In order to obtain initial values for the particle diameter, the velocity and the temperature, measurements were done. Velocity and diameter are measured with help of a newly developed particle diagnostics system, the particle shape imaging (PSI) [7, 16] and moreover by use of particle image velocimetry [2], while the surface temperature measurements are obtained by spectroscopic methods [8].

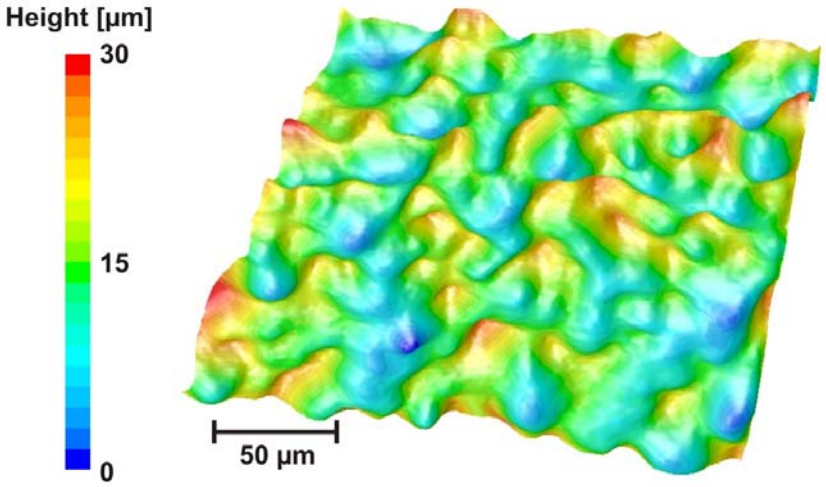

Figure 1. Simulation of a grid blasted substrate

2.1.3. Computational grid and boundary conditions

An example of the computational grid can be found in Fig. 2. The blue colored surfaces indicate the outlets. They are defined as pressure-outlets at operating pressure with a total backflow temperature of about 700 K. At the dark red colored surface a wall boundary is used, which represents the surface. In the case of the first flattening particle, only the steel surface has to be considered. Afterwards one has to distinguish, whether the wall consists of the steel substrate or of a formally solidified alumina particle.

The cylindrical zones in the grid indicate the initial positions of the particles, just before impinging. This kind of geometry was chosen, in order to minimize the number of cells in the grid. With help of sample calculations it could be ensured that such a grid geometry delivers pretty good approximations, because the gas flow shows no significant influence. By use of this kind of grid geometry the total number of cells could be decreased from approximately 5 million cells to about 2 million cells, which significantly reduces the calculation time.

The computational grid, used in the simulations was made out of tetra elements. These elements have an average size from about 1 micron up to about 3 microns, depending on the position in the grid. The regions, where the flattening and solidification of the particles takes place, are meshed with smaller element sizes, while in regions, where no significant velocity and pressure changes are expected, the element size is increased up

to three times. Fig. 3 shows a cross section of the grid. Here the cell size distribution can be seen.

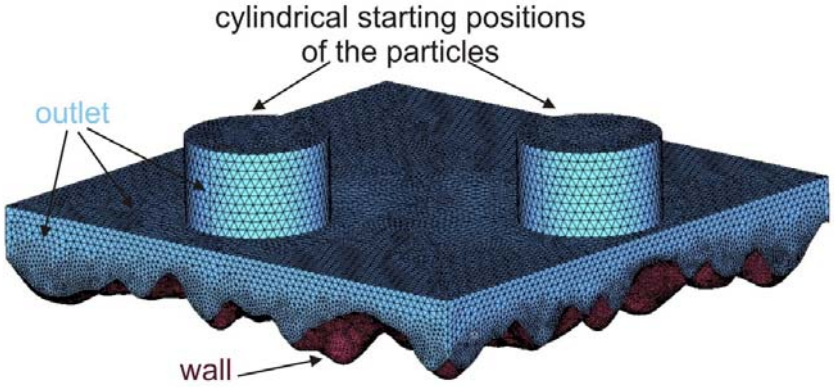

Figure 2. Example of a computational grid for CFD calculations

In the calculations the PISO algorithm was used for pressure-velocity coupling. On the basis of past experience it could be shown, that a fixed time stamp of 5.0 e^{-10} s is the most suitable solution, in order to obtain stable results. In Fig. 4 the velocity field of a flattening particle onto already solidified particles is shown. Fig. 4a illustrates the initial position of the particle at the start of the calculation. The initial velocity magnitude was 150 m/s in negative vertical direction. In Fig. 4b the flattening process has almost finished. The flow time at this point is 0.5 µs. These calculations were carried out with the commercial CFD software Fluent.

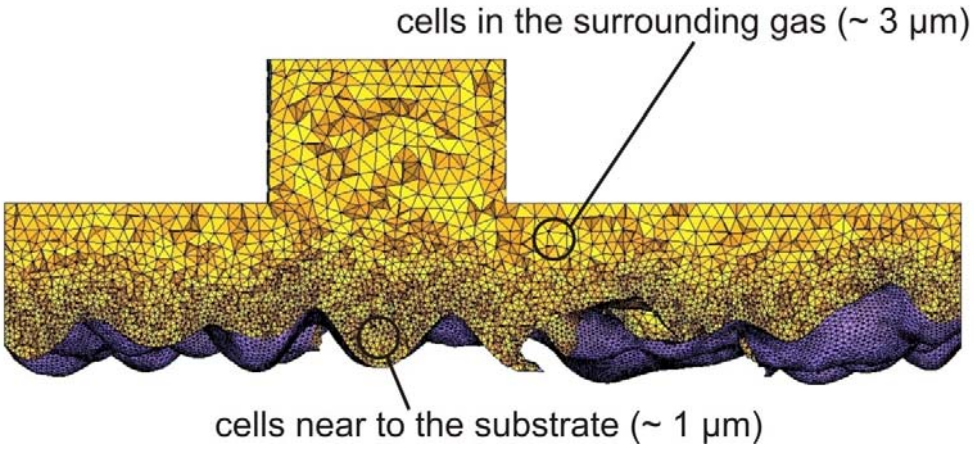

Figure 3. Cross section of a computational grid, showing the cell size distribution

2.2. Coupling of CFD and FEM

As to be seen in Fig. 4, with use of CFD the flattening process of the particles can be successfully calculated. The effects that occur due to cooling down of the particle, e.g. the shrinking of the particles and the constitution of micro pores, cannot be treated with CFD. On the other hand, experimental investigations of the coating properties indicate, that these effects have a significant influence. In order to accomplish the coupling of CFD and FEM, the steps, figured out in Fig. 5 have to be realized. Beyond the parameters that directly result of the CFD-calculation, the most important task is to carry out a contact definition

between particle and substrate or rather between two colliding particles. This contact definition is dependent on:

1. the contact time
2. the temperature difference between particle and bedrock
3. the distance between particle and bedrock

The so called contact time is the minimal time frame, which is needed that diffusion processes with the substrate material can take place.

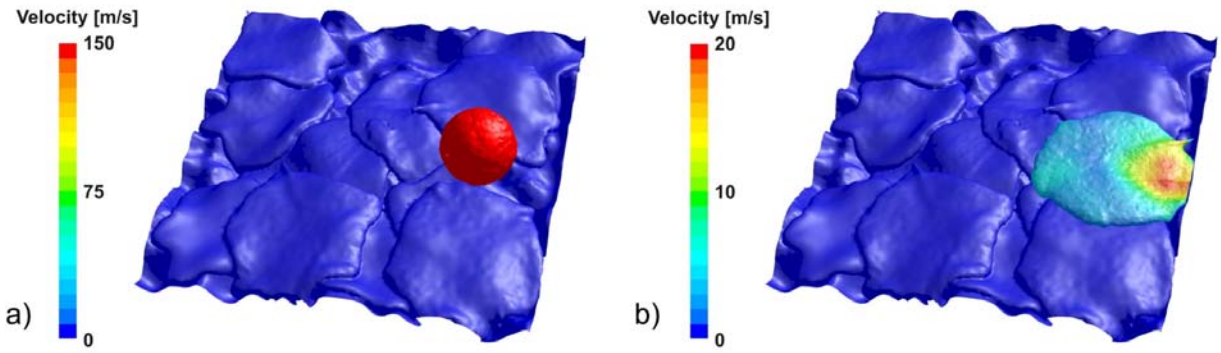

Figure 4. Velocity fields of a flattening particle

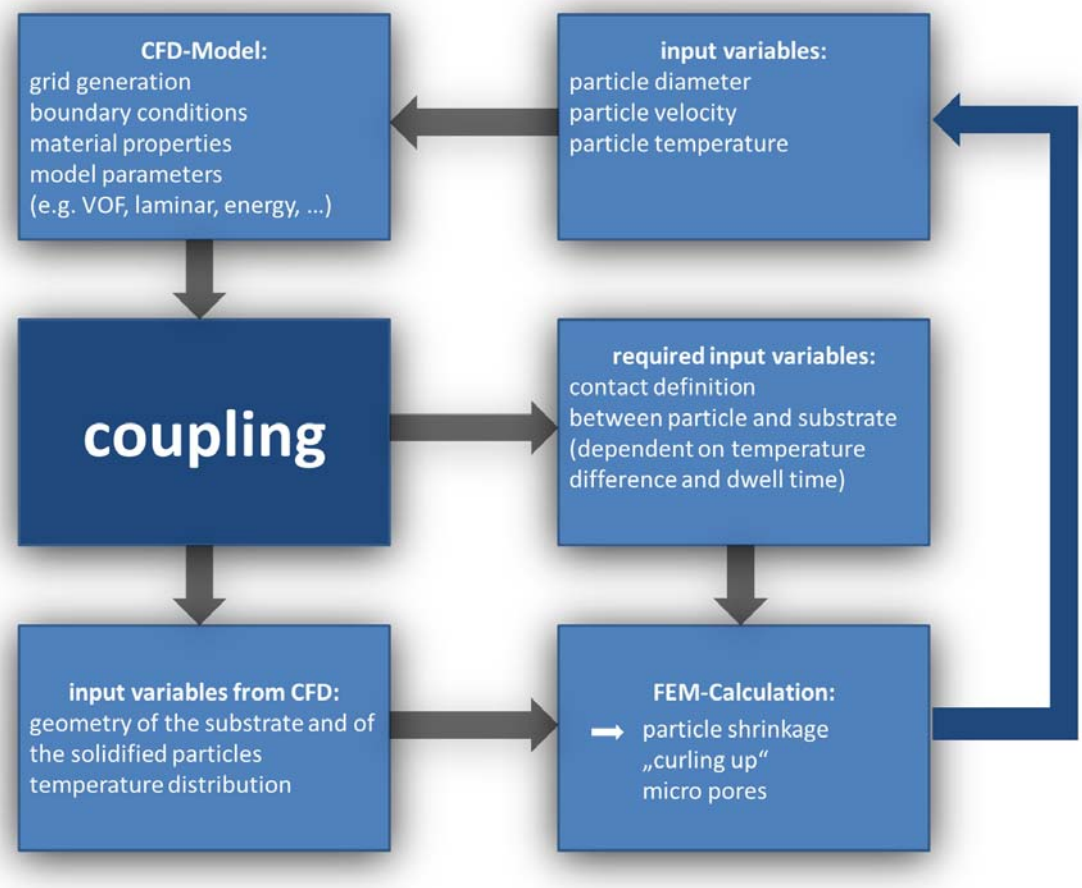

Figure 5. Schematic of the coupling procedure

These above-mentioned parameters have to be obtained out of the CFD-calculation. For this reason, the CFD-model was modified. A new primary zone in the fluid regime of

the grid was created (see Fig. 6). This zone, which is positioned at the bottom layer of the grid, is the only area, where contact between the particle and the bedrock is possible. This newly created zone is analyzed after every time step and the parameters: volume fraction of the particle, temperature and flow time are written to a file, so that they can be processed afterwards. Fig. 7 shows a front view of the substrate with contact areas at different contact times. In the red colored areas, the conditions for the specific contact definitions are met. The contact time in Fig. 7a is
e^{-8} s, while the contact time in Fig. 7b was chosen as 5.0 e^{-8} s. Which value is the most realistic one, must be compared with experiment.

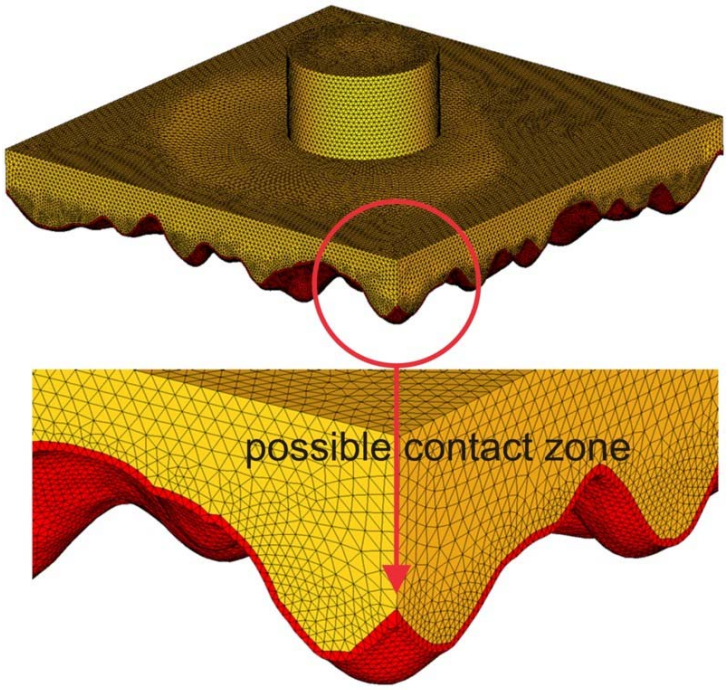

Figure 6. Possible contact zone

Once the contact areas are defined, the FEM-calculation can be set up. First of all, the shape of the flattened particle has to be extracted out of the CFD grid. In order to transfer this shape into a Finite Element volume mesh, the commercial meshing tool Hypermesh was used.

During the FEM-calculations, the heat transfer in the substrate in thickness direction is not modeled. In order to justify this, the thermal diffusion distance was estimated. The thermal diffusion distance can be defined as:

$$s_d := \sqrt{\alpha_{th}\, t_c} \tag{9}$$

With typical values of $\alpha_{th} = 1e^{-6}$ m²/s and $t_c = 1e^{-7}$ s, the thermal diffusion distance can be estimated to $s_d = 3e^{-7}$ m. Due to the fact, that this value is significantly smaller than the average cell height of about one micron, the heat transfer was neglected.

After the FEM-calculation has finished, the newly generated “shrinked” particle shape has to be re-imported into the CFD grid, where it is now part of the surface with the thermal properties of alumina.

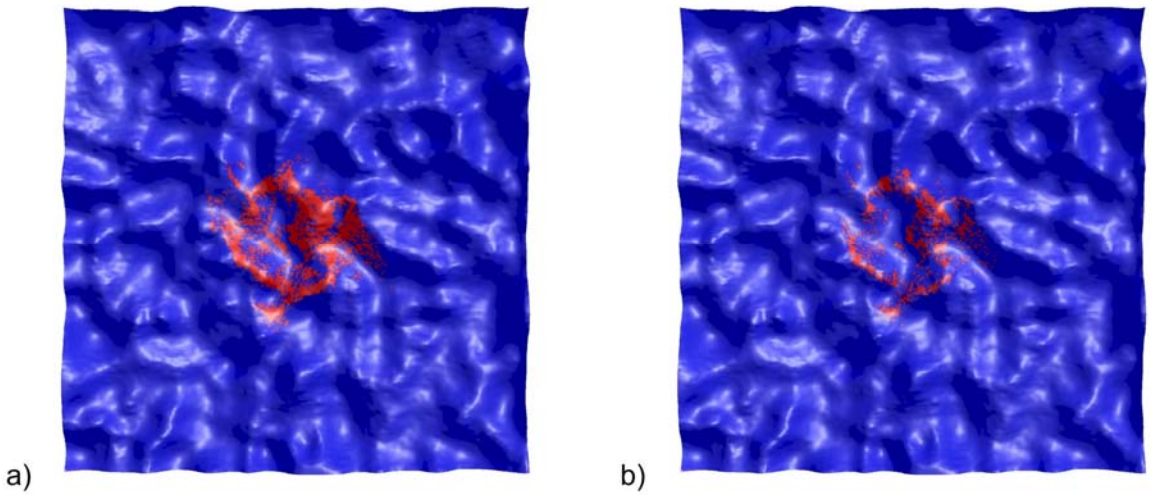

Figure 7. Contact definition at different contact times, a) 1.0 e^{-8} s; b) 5.0 e^{-8} s

3. Results

The FEM calculations were done with the FEM software Abaqus. As a result, one can see in Fig. 8 the shrinking of a particle due to cooling down. The maximum displacement due to cooling down is about 1 micron. Since the average height of a flattened particle is about the same dimension, this result demonstrates the importance of FEM calculations at coating formation simulations. Moreover the curling up of the particle edges can be observed, Fig. 8.

Most of the bottom side of the flattened particle is bonded to the substrate, so that it cannot contract. On the other hand, the upper surface shrinks, which causes the edges to curl up. The curling up of the edges is up to one micron in the vertical direction. Hence this effect has a significant influence to the formation of micro pores.

In the field of Thermal spraying, curling up is a well known effect. In [14] this effect is investigated at single molten metal drops. In addition to the experiment an analytical model of curl-up angle is presented.

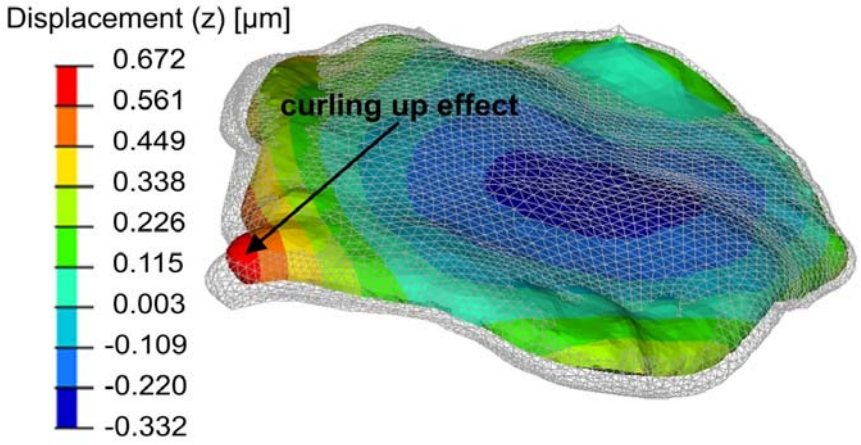

Figure 8. Particle shrinking and curling-up due to cooling down

The constitution of micro pores is an interplay between the shrinking effects as described above and the fact that the mold filling during spreading is not completely guaranteed. Fig. 9 shows such micro pores witch are formed throughout the process of spreading and cooling down.

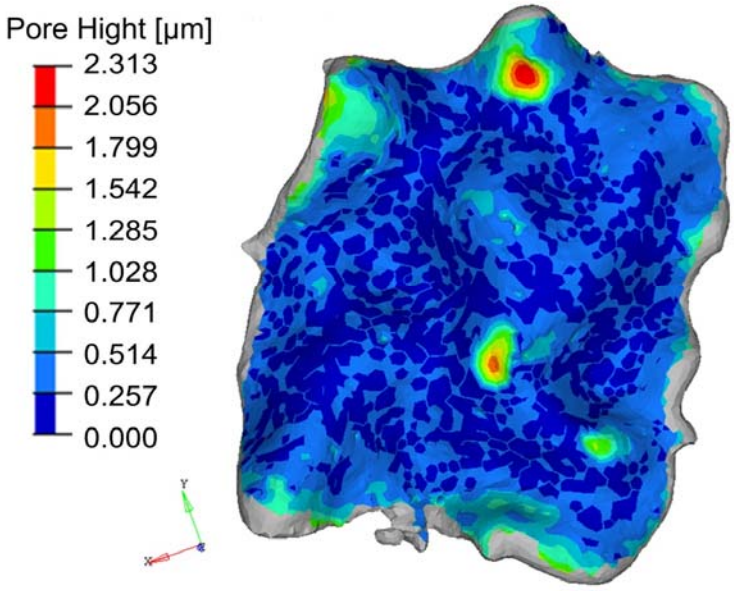

Figure 9. Pores at the background of a particle

A verification of the simulation can best be determined by use of cross sections, obtained from real coatings. The steel specimen was coated using a triple-cathode plasma torch [1]. The spray powder was alumina having a particle size of 22 µm to 45 µm. In Fig. 10, a comparison of experiment and simulation is illustrated. The diverse colours indicate different particles. Both, the pore content and size as well as the particle shapes are in good qualitative agreement.

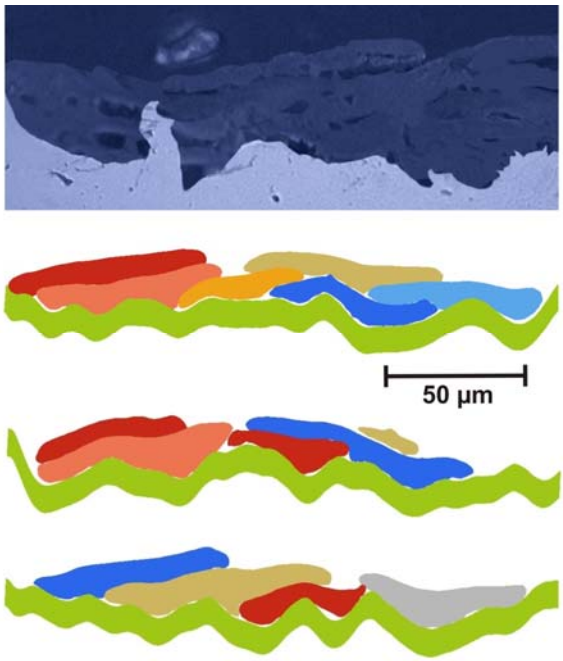

Figure 10. Comparison of experiment and simulation

4. Conclusion

The goal of the simulations, shown in this paper, is to improve coating formation simulations in the field of Thermal Spraying with respect to shrinking effects and the occurrence of micro pores due to cooling down. Here, a coupled CFD and FEM calculation is presented. With use

of CFD, the flattening and the solidification of the particles is simulated, while the Finite Element Method is used in order to simulate the shrinking effects. Due to the fact that the time between two successive particle impacts at the same place is statistically greater than the solidification time of the first particle, the separate treatment of the two processes is possible. It could be shown, that this procedure has a significant influence on the resulting coating properties, hence the micro pores are of the same dimension as the height of the flattened particles.

In future work, we plan to expand the model and to scale it up, so that it will be possible to simulate macroscopic coatings. This results in the fact that the simulations can be compared with real coatings in a better way.

Acknowledgement

The authors gratefully acknowledge the German Research Foundation (DFG) for the financial support within the project bundle "Homogenization of Coating Properties in Atmospheric Plasma Spraying" (PAK 193), and especially for the support of the subproject "Simulation of the structure of coatings, which are sprayed by use of 3-cathode plasma spraying" (BA 851/92-1).

Nomenclature

α_p	Cell based volume fraction of the particle	σ	Surface tension
α_g	Cell based volume fraction of the gas	α_{th}	Thermal diffusity
ρ_p	Particle density	t_c	Contact time
$\vec{v}_p$	Cell based velocity vector of the particle	s_d	Thermal diffusion distance
f	Cell based number of faces	P	Pressure
U_f	Volume flux through the face	E	Energy
Δt	Time step	λ	Thermal conductivity
$\alpha_{p,f}$	Face value of the volume fraction	T	Temperature
V	Cell volume	T_m	Melting temperature
E	Energy	σ	Surface tension
λ	Thermal conductivity	α_{th}	Thermal diffusity
T	Temperature	t_c	Contact time
T_m	Melting temperature	s_d	Thermal diffusion distance

References

[1] Bach, F.W., Möhwald, K., Laarmann, A. and Wenz, T. (editors) Modern Surface Technology, chapter Triplex II - Development of an Economical High-performance Plasma Spray System, pages 168–178. WILEY, 2006.

[2] Bach, F.W., Möhwald, K., Rothardt, T., Prehm, J., Engl, L., Hartz, K. and Drößler, B. Particle image velocimetry in thermal spraying. Materials Science and Engineering A, 383(1):146–152, 2004.

[3] Beauvais, S., Guipont, V., N'Guyen, F., Jeandin, M., Jeulin, A., Robisson, D. and Saenger, R., Study of the porosity in plasma-sprayed alumina through an innovative 3-dimensional simulation of the coating build-up. Proc. International Thermal Spray Conference, 2004.

[4] Bussmann, M., Chandra, S. and Mostaghimi, J., Numerical results of off-angle thermal spray particle impact. Proc. UTSC, Düsseldorf, Germany, pages 783–786, 1999.

[5] Fluent_Inc. Fluent 6.3 user's guide.

http://my.fit.edu/itresources/manuals/fluent6.3/help/html/ug/main_pre.htm.

[6] Hirt C.W. and Nichols, B.D. Volume of fluid (vof) method for the dynamics of free boundaries. Journal of Computational Physics, 39:201–225, 1981.

[7] Landes, K., Diagnostics in plasma spraying techniques. Surface and Coatings Technology, 201(5): 1948–1954, 2006.

[8] Mauer, G., Vaßen, R. and Stöver, D., Comparison and applications of dpv-2000 and accuraspray-g3 diagnostic systems. Journal of Thermal Spray Technology, 16(3):414–424, 2007.

[9] Raessi, M., Mostaghimi, J. and Bussmann, M., Impact and solidification of droplets onto rough substrates. Proc. International Thermal Spray Conference, 2005.

[10] Steinke T. and Bäker, M., Simulation of thermal sprayed coatings, Proc. International Thermal Spray Conference, 2006.

[11] Voller V.R. and Prakash, C., A fixed-grid numerical modeling methodology for convection-diffusion mushy region phase-change problems. Int. J. Heat Mass Transfer, 30(8):1709–1719, 1987.

[12] Voller, V.R. and Swaminathan, C.R. Generalized source-based method for solidification phase change. Numer. Heat Transfer B, 19(2):175–189, 1991.

[13] Wan, Y.P., Prasad, V., Wang, X.G., Sampath, S. and Fincke, J.R., Model and powder particle heating, melting, resolidification, and evaporation in plasma spraying processes. Journal of Heat Transfer - Transactions of the ASME, 121:691–699, 1999.

[14] Xue, M., Chandra, S., and Mostaghimi, J. Investigation of splat curling up in thermal spray coatings. Journal of Thermal Spray Technology, 15:531–536, 2006.

[15] Xue, M., Mostaghimi, J. and Chandra, S. Prediction of coating microstructure. Proc. International Thermal Spray Conference, 2004.

[16] Zimmermann, S. and Landes, K. A particle image shape imaging (psi) investigation of particles in a plasma jet. Materials Science and Engineering A, 383(1):153–157, 2004.

[17] Paradis, P.F. and Ishikawa, T. Surface Tension and Viscosity Measurements of Liquid and Undercooled Alumina by Containerless Techniques. Japanese Journal of Applied Physics, 44(7A):5082–5085, 2005.